



# Numerical simulation and aeroacoustic noise modelling of a wind turbine using a blade section in an annulus

Sahan Hasaranga WASALA<sup>1</sup>; Stuart Edward NORRIS<sup>2</sup>; John Edward CATER<sup>3</sup>

<sup>1,2,3</sup> University of Auckland, New Zealand

## ABSTRACT

Noise disturbance from wind turbines is one of the major factors which slows wind farm development near populated areas. Therefore, it is important to have an accurate estimate of the noise generated before production and installation of wind turbines. Large Eddy Simulation (LES) can be used to determine the aerodynamic sound produced by a moving surface, but LES of a whole wind turbine is computationally expensive. However, Oerlemans' field measurements show that most of the noise from wind turbines is generated at 75%-95% of the span of the blade. This suggests that simulation of a section with the most significant noise sources could lead to a useful overall noise estimate in the far field. The present work is focused on noise prediction from a wind turbine using a rotational annulus containing a section of a wind turbine blade, which leads to a significant reduction of computational expense. LES with the Ffowcs-Williams and Hawkings acoustic analogy is used to predict the far field acoustic noise. Initial results with rotational CART-2 wind turbine blade show good agreement with the available experimental data.

Keywords: Noise, Wind turbine, Aeroacoustic I-INCE Classification of Subjects Number(s):14.5.4, 76.9

## 1. INTRODUCTION

Wind turbines are one of the main resources of renewable energy with a great potential to replace limited fossil fuel based energy sources. In an increasingly urbanised world, it is difficult to avoid wind farms near human habitat. Studies by Salt (1) and Nissenbaum (2) show that the noise generated from wind turbines has adverse physical and psychological health effects to the people living nearby. Therefore, it is important to estimate the noise levels before installation and find possible ways to reduce it.

Wind turbine noise can be categorised into two major sources based on the sound generation mechanism; mechanical noise and aerodynamic noise. Mechanical noise is mainly due to moving parts inside the gear box and the generator (3). This source of noise is able to be reduced through technologies such as high precision gear tooth profile designs and acoustic insulation of the nacelle (4). However, aeroacoustic sources are more complex and not easy to control.

Aeroacoustic sources can be defined as monopole, dipole and quadrupole sources. Monopole and dipole sources originate near surfaces and are strong radiators of the acoustic energy (5). Quadrupole sources originate far from surfaces and are weak radiators (6). The aerodynamically generated noise from a wind turbine is due to the unsteady loading mainly on the surface of the wind turbine blade, resulting strong monopole and dipole sources. These sources can be resolved using Computational Fluid Dynamic (CFD) and Computational Aeroacoustic methods (CAA). An accurate estimation of the noise generation from a wind turbine requires well resolved flow field data, especially near the surface of the blade. This is computationally expensive to model in CFD since it requires a fine computational grid around the surface of the blade and leads to higher temporal resolution requirements for transient simulation in order to avoid numerical instability. However, the acoustic camera measurements of Oerlemans et al. (7) suggest that the majority of the noise sources are located at the 75%-95% span section of the wind turbine blade, where the local flow velocities are relatively high. Simulating only this region of the blade could reduce the computational cost compared to a full wind turbine simulation, and may produce sufficient acoustic source data for accurate far field noise prediction.

In the present work, the flow field around a rotational wind turbine blade is simulated using LES with ANSYS Fluent (8). The Ffowcs-Williams and Hawkings acoustic analogy is used to calculate the acoustic

<sup>1</sup>s.wasala@auckland.ac.nz

<sup>2</sup>s.norris@auckland.ac.nz

<sup>3</sup>j.cater@auckland.ac.nz

pressure at a far field receiver location.

## 2. BACKGROUND

### 2.1 Aeroacoustic noise generation mechanisms

In 1983, Brooks et al. (9) introduced two main aeroacoustic broadband noise generation mechanisms for rotating aerofoil sections. The first is the turbulent ingestion noise, which is a function of inflow turbulence. The second noise mechanisms is the aerofoil self-noise which is a function of the blade geometry. The aerofoil self-noise generation can be categorised as turbulent boundary layer trailing edge noise, laminar boundary layer vortex shedding noise, separation and stall noise, trailing edge bluntness and vortex shedding noise and tip vortex noise. Detailed explanation of the noise sources can be found in (10). In addition to the noise generation mechanisms discussed above, wind turbines have a mechanism due to rotation of the blade and the interaction between the wake with the tower. This noise mechanism has a tonal character where the tones are at integer multiples of the blade passing frequency of the rotor (11) and is neglected in the present study in order to keep the computational cost to a minimum. The low frequencies in the acoustic noise spectrum are mainly due to the turbulence inflow (12), and are difficult to determine because of the chaotic character of the turbulence flow.

Schlinker and Amiet (13) identified the trailing edge noise as the main noise source from a rotor. Moriarty (16) developed a semi-empirical wind turbine noise prediction method based on Brooks' work (10). However his predicted noise levels differed from the experiment data. Recent studies by Mo et al. (14) used LES to simulate the aeroacoustic noise from the NREL phase VI wind turbine. However, they did not investigate frequencies in the range of 1 to 5 kHz, for which the human ear is most sensitive. Arakawa et al. (15) simulated the noise from the WINDMELIII wind turbine using LES. However, this work does not have a good quantitative validation, where the results largely differ, especially due to the insufficient span-wise grid points. Orlemans (7) field noise measurements show that the major noise sources start at about 75% of the span of the blade and most of the energy is below 1 kHz. At approximately 95% span, frequencies above 1 kHz have high energy, though less amplitude with respect to low frequency inboard sources. From this data we propose that the noise generated at inboard region of the blade can be neglected. Therefore in the present work an annular section of the 75%-95% span of the CART-2 wind turbine blade is simulated, with the assumption that all of the noise sources are located at that region. Additionally it is assumed that there is no radial flow at the inner and outboard sections of the blade.

### 2.2 Large Eddy Simulation

The flow around a wind turbine is highly turbulent (16). For an accurate calculation of the flow field, especially for an aeroacoustic problem, it is necessary to use methods such as Direct Numerical Simulation (DNS) or Large Eddy Simulation (LES). LES is computationally less expensive than DNS, and to date has shown reasonable results for acoustic simulations (17).

Large scale turbulence in a flow can have a complex and anisotropic structure. However, small scale eddies may assumed to be isotropic. In LES, a low-pass-filter is used to filter the Navier-Stokes equations, and the small length scales, less than the filter width, are modelled using a sub-grid scale turbulence model. The sub-grid scale model used in this study is that of Smagorinsky (18) and Germano (19).

The unsteady filtered three dimensional Navier-Stokes equation can be written as follows. Where, the mass continuity equation is,

$$\frac{\partial \rho}{\partial t} + \frac{\partial}{\partial x_i}(\rho \bar{u}_i) = 0, \quad (1)$$

and the conservation of momentum equation is,

$$\frac{\partial}{\partial t}(\rho \bar{u}_i) + \frac{\partial}{\partial x_j}(\rho \bar{u}_i \bar{u}_j) = \frac{\partial}{\partial x_j}(\sigma_{ij}) - \frac{\partial \bar{p}}{\partial x_i} - \frac{\partial \tau_{ij}}{\partial x_j}, \quad (2)$$

where,  $\sigma_{ij}$ , the stress tensor due to molecular viscosity is,

$$\sigma_{ij} \equiv \left[ \mu \left( \frac{\partial \bar{u}_i}{\partial x_j} + \frac{\partial \bar{u}_j}{\partial x_i} \right) \right] - \frac{2}{3} \mu \frac{\partial \bar{u}_l}{\partial x_l} \delta_{ij}, \quad (3)$$

and subgrid scale stress is defined by  $\tau_{ij}$ , where,

$$\tau_{ij} \equiv \rho \overline{u_i u_j} - \rho \bar{u}_i \bar{u}_j. \quad (4)$$

The subgrid scale stresses are modelled using the Boussinesq hypothesis (17),

$$\tau_{ij} - \frac{1}{3}\tau_{kk}\delta_{ij} = -2\mu_t\bar{S}_{ij}, \quad (5)$$

where,  $\mu_t$  is the subgrid-scale turbulent viscosity. The isotropic part of the sub-grid scale stress  $\tau_{kk}$  is not modelled, but added to the filtered static pressure term. The rate of strain tensor,  $\bar{S}_{ij}$  is,

$$\bar{S}_{ij} \equiv \frac{1}{2}\left(\frac{\partial\bar{u}_i}{\partial x_j} + \frac{\partial\bar{u}_j}{\partial x_i}\right), \quad (6)$$

and the eddy viscosity is  $\mu_t$  is modelled by,

$$\mu_t = C_s\Delta^2|\bar{S}|, \quad (7)$$

where,  $C_s$  is the Smagorinsky constant and  $\Delta$  is the subgrid filter width which is,

$$\Delta = V^{\frac{1}{3}}, \quad (8)$$

where  $V$  is the local cell volume and,

$$|\bar{S}| \equiv \sqrt{\bar{S}_{ij}\bar{S}_{ij}}. \quad (9)$$

In the present work the Smagorinsky constant is calculated dynamically using the method first implemented by Germano (19). A test filter is used, where the filter width is as twice the grid filter width. Both filters produce a resolved flow field. The information from the filters are used for calibration of the model constant  $C_s$ .

### 2.3 Acoustic Simulation

The earliest approach to formulate the aeroacoustic noise was that of Lighthill in (6, 20), where he rearranged the Navier-Stokes equation into a inhomogeneous wave equation given by,

$$\frac{\partial^2\rho}{\partial t^2} - c_0^2\nabla^2\rho = \frac{\partial^2 T_{ij}}{\partial x_i\partial x_j}, \quad (10)$$

where,  $c_0$  is the speed of the sound. The right hand side represents the quadrupole source term, where Lighthill's stress tensor  $T_{ij}$  is,

$$T_{ij} = \rho v_i v_j - \sigma_{ij} + (p - c_0^2\rho)\delta_{ij}. \quad (11)$$

The left hand side of eq. 10 describes the propagation of the acoustic wave in both spatial and temporal domains. The purpose of derivation of this equation was to predict aircraft jet noise, which was a major concern when civil aviation become a common form of transportation. Lighthill only considered quadrupole sources, which are the main source of jet noise. Later, Ffowcs-Williams and Hawkings (FW-H) (21) extended Lighthill's equation, to allow to prediction of noise from a moving surface. The FW-H equation has two extra source terms which represent monopole and dipole sources, shown in eq. (12). When  $p' = c_0^2\rho'$ ,

$$\begin{aligned} \frac{1}{c_0^2}\frac{\partial^2 p'}{\partial t^2} - \nabla^2 p' &= \frac{\partial^2}{\partial x_i\partial x_j}\{T_{ij}H(f)\} \\ &- \frac{\partial}{\partial x_i}\{[P_{ij}n_j + \rho u_i(u_n - v_n)]\delta(f)\} \\ &+ \frac{\partial}{\partial t}\{[\rho_0 v_n + \rho(u_n - v_n)]\delta(f)\}, \end{aligned} \quad (12)$$

where  $p'$  is the acoustic pressure at the far field and  $f$  is the mathematical surface of the moving body. Solving the FW-H equation at every grid point on the domain requires a fine computational grid and is computationally expensive. However, the solution at an interested receiver location can be calculated using generalised function theory and free space Greens function, where the solution to the wave equation is known (22). The detailed derivation of eq.13 can be found in (23). The method assumes that there are no obstacles between the source and the receiver which could disturb the acoustic wave. The acoustic wave is also assumed to exert no forces on the fluid flow. Additionally, in this simulation, the weak quadrupole sources are neglected from the calculation, as they are be assumed to have no significant acoustic contribution to a far-field receiver. The surface stresses are assumed to be negligible for subsonic flow.

$$4\pi p'(x,t) = \frac{1}{4\pi}\frac{\partial}{\partial t}\int_{f=0}\left[\frac{\rho_0 v_n}{r(1-M_r)} + \frac{p\cos\theta}{c_0 r(1-M_r)}\right]_{ret} ds + \int_{f=0}\left[\frac{p\cos\theta}{r^2(1-M_r)}\right]_{ret} ds, \quad (13)$$

where,  $M_r$  is the Mach number of a point on the moving surface,  $\theta$  is the local angle between normal to the surface and radiation direction,  $r$  is the distance to the observer. The right hand side of eq. (13) contains the monopole and dipole sources, where  $f$  is the moving surface. The left hand side gives the acoustic pressure at the receiver location. This method has been widely used to predict the noise generation from helicopter rotors. For instance, the WOPWOP and PSU WOPWOP (24) codes have shown accurate predictions using this method.

### 3. METHODOLOGY

The methodology for the wind turbine blade simulation is initially tested on a NACA0012 aerofoil in a rectangular domain and validated with experiment data by Brooks et al. (10). The simulation strategy can be summarised as shown below.

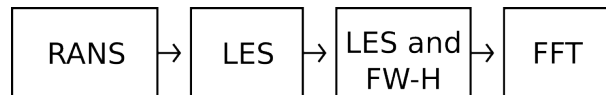


Figure 1 – The simulation strategy for obtaining and processing the acoustic data.

#### 3.1 Mesh generation

The domain size was scaled such that the blockage ratio of the NACA0012 blade is less than 1%. The geometry of the NACA0012 is designed in ANSYS ICEM CFD (25) with a sharp trailing edge, since the wind tunnel experiment had a trailing edge thickness of less than 0.016% of the chord. The chord of the chosen case is 0.3048 m. A hybrid computational grid was created using ICEM. The boundary layer thickness at the trailing edge was estimated using the Blasius equation and is spanned by 12 structured prism layers. The region in the downwind direction, where the wake is expected, was also refined. Wall  $y^+$  is order one (17). The span-wise and chord-wise surface grid size are kept equal ( $\Delta x = \Delta z$ ). Outside the structured surface mesh, another 5 uniform size tetrahedral layers were included. In the far field mesh, the maximum cell size was limited to less than 1/3 of the span. A mesh resolution study was performed in order to obtain a solution independent mesh. A minimum number of 152 points along the chord of the blade was required for good agreement with experimental data.

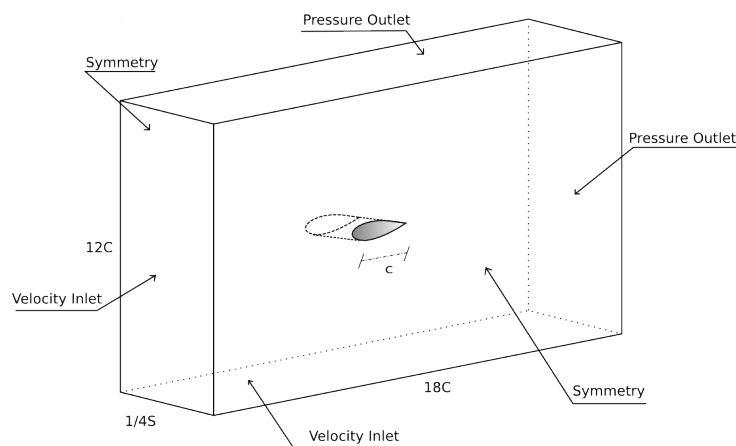


Figure 2 – Rectangular domain of the initial NACA0012 simulation.

#### 3.2 Boundary conditions

Two of the boundaries were inlets with a prescribed velocity of 71.3 m/s, and the other two as outlets with a prescribed zero gauge pressure, to simulate the uniform flow in the far field. The two sides of the domain were simulated with symmetrical boundary conditions.

#### 3.3 Steady state solution

A steady state RANS (Reynolds-averaged Navier–Stokes equations) solution has been used for the initial flow field for the LES simulation. In this way the transient flow field reached a quasi-steady state more rapidly than initialising the flow field with a uniform velocity, significantly reducing the computational cost of the LES calculation. The RANS solution was calculated with the Fluent SIMPLE solver, using third order spatial

differencing, with the convergence criteria of  $10^{-6}$ .

### 3.4 Transient solution

The iterative PISO algorithm was used for the transient LES, with the pressure and momentum equations solved using a second order central differencing scheme. A Green-Gauss node-based method is used to evaluate the pressure gradient (26). The optimal time step size was found with a temporal resolution study. A time step size of  $10^{-6}$  s provided a stable solution with the Courant number throughout the domain being less than 0.3. The simulation became quasi-steady after a single flow domain pass-through and data from a subsequent pass-through was used for post processing.

### 3.5 Acoustic solution

The blade surface pressure data is used to calculate the acoustic surface sources at every time step. After the transient flow simulation these values were used to calculate the acoustic pressure at a given receiver location in the acoustic far field. The Doppler effect due to a uniform free stream flow is accounted for in the calculation. The final raw acoustic pressure data post processed using Fast Fourier Transformation (FFT) based on Welch's power spectral density estimation method with a Hamming windowing function (27). A 1/3 octave spectra is used to compare results with experimental data.

## 4. VALIDATION

### 4.1 Flow field

The time averaged lift coefficient has been evaluated for LES calculations at four different angles of attack, and agrees well with the experimental data of Abbott and Doenhoff (28). The mesh for this validation consisted of 3.2 million nodes, the free stream velocity was 71.3 m/s, which results in a Reynolds number of  $1.5 \times 10^6$ .

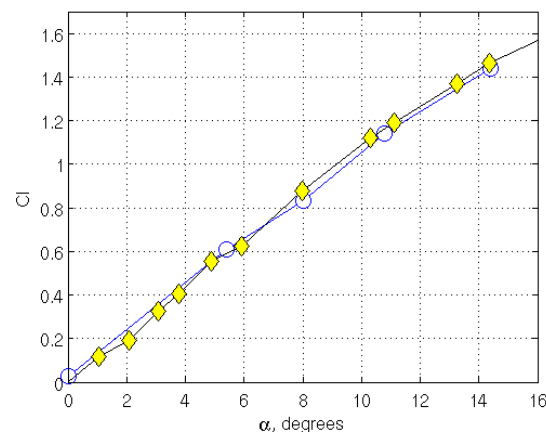


Figure 3 –  $C_L$  CFD results (○) compared with experimental data (◇) from Abbott and von Doenhoff (28).

### 4.2 Acoustic results

An acoustic receiver was located at a point in the mid-span plane 1.2 m behind the trailing edge of the blade, perpendicular to the chord line. The 1/3 octave spectra of the numerical results is compared with the experimental data of Brooks et al (10). The results, as shown in Figure 4, show good agreement especially at high angles of attack. A spectral hump at approximately 5 kHz is observed at  $\alpha = 0^\circ$  and  $\alpha = 5^\circ$  which diverge from the experiment data and is still under investigation.

As the angle of attack increases, the main peak of the spectral hump moves to lower frequencies, i.e. noise at low frequency increases. This did not have any significant effects on the energy at high frequencies. Overall, the method proved to give a good prediction of the far field noise.

## 5. CART-2 WIND TURBINE BLADE SIMULATION

The two bladed Control Advanced Research Turbine (CART-2) is located at the National Wind Technology centre (NWTC) in Boulder, Colorado, and is a Westinghouse 600 kW horizontal axis wind turbine with a 42 m rotor diameter (D) and 36.6 m hub height (H). The CART-2 wind turbine blade consists of a LS(1)-04XX aerofoil section, where the chord and the aerofoil thickness varies with respect to the span. Acoustic measurements of this wind turbine have been made by Moriarty (16) according to the IEC61400-11 standard, where the receiver located at ground level at a distance  $H + D/2$  in the downwind direction. The initial

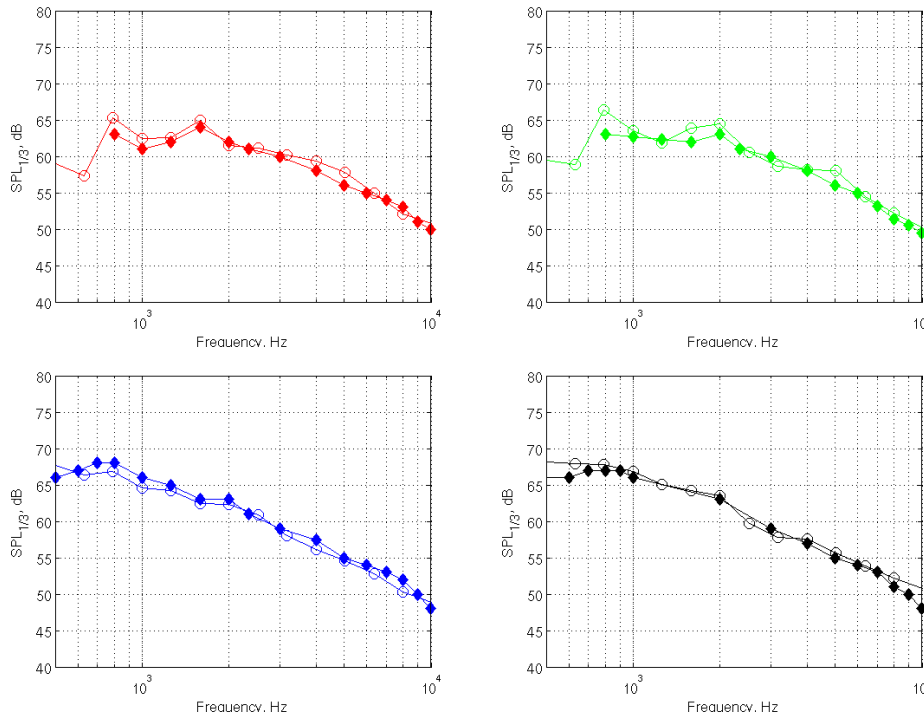


Figure 4 – Anechoic wind tunnel acoustic measurement data for NACA0012 aerofoil at  $\alpha = 0^\circ$  ( $\blacklozenge$ ),  $5.4^\circ$  ( $\blacklozenge$ ),  $10.8^\circ$  ( $\blacklozenge$ ) and  $14.4^\circ$  ( $\blacklozenge$ ). Numerical results are shown with open symbols.

simulation was conducted for the case where the blade pitch angle was  $3^\circ$ . The mean inlet velocity at hub height is 10.81 m/s and the turbulent intensity at the inlet is 10.3%. The rotational velocity is 41.8 rpm and is constant during the simulation.

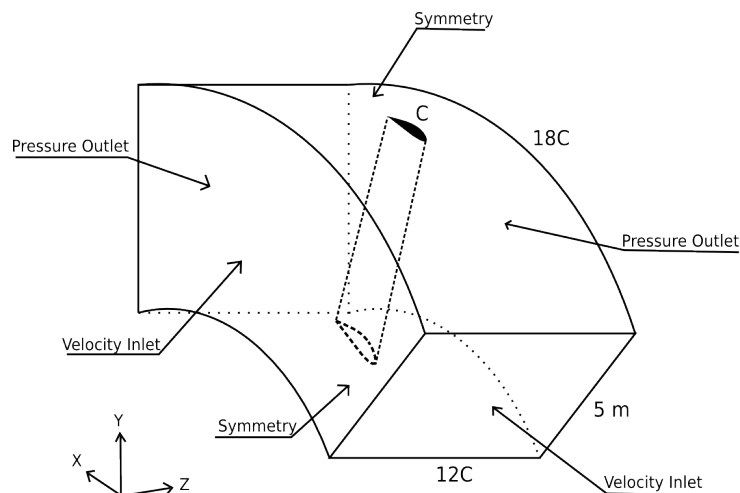


Figure 5 – A section of the CART-2 blade in an annular domain.

The dimensions of the annular domain are similar to the rectangular domain with respect to the tip chord length. The mesh is generated with the same cell distribution as described in section 3.1, with the number of grid points per chord kept at 152. This reduced the acoustic resolution of the computation down to 4.5 kHz when a second order method is used for spatial discretisation. In addition to the boundary conditions specified for the rectangular domain, a rotational reference frame was used to simulate the rotation of the blade with constant rotational velocity.

## 6. RESULTS AND DISCUSSION

The computational mesh for the rotational simulation consisted of 15.8 million cells. The simulation was stable at a transient time step of  $5 \times 10^{-6}$  s, and ran for 0.1175 s, in which time the blade rotated by approximately  $30^\circ$ . This calculation took about 10 days running parallel on 128 cores. Due to the lack of the data for a whole rotation, 12 receivers were located on a circle of radius  $H$  at 58 m downwind of the blade. This enabled the simulation of a complete  $360^\circ$  rotation. The final raw acoustic data was post processed and the results are presented in Figure 6.

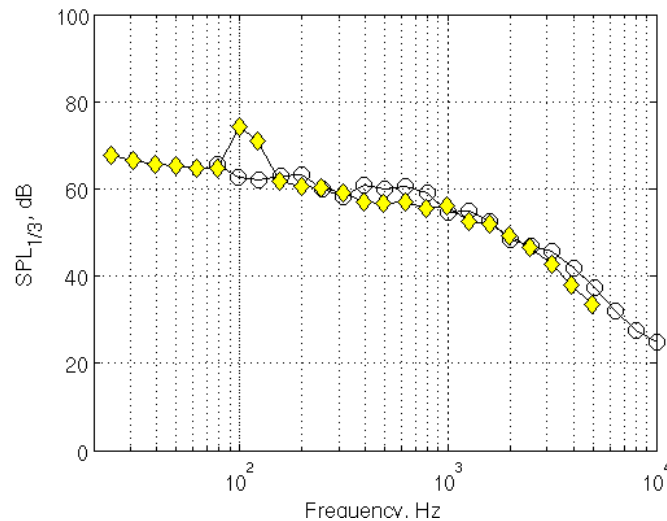


Figure 6 – Comparison of simulated CAA results (○) with the acoustic field measurements (◇) by Moriarty (16).

The acoustic spectrum of the numerical simulation is in good agreement with the experimental data. A peak at approximately 100 Hz is not evident in the numerical results. Moriarty (16) suggested that this peak could be due to mechanical noise, which may account for this discrepancy. There is another small peak at approximately 1 kHz in the experimental data which is not shown in the numerical result. Comparing with Moriarty's semi-empirical code, this peak could be due to the bluntness of the trailing edge of the blade. The current blade used in the simulation is sharper than the LH(1)-04XX used in CART-2. This will be investigated in future work. There are two spectral humps shown in the numerical results. The first is at 150 Hz-300 Hz, and the second is at 400 Hz-800 Hz. These humps are thought to be related to the length scales of the inflow turbulence. This will also be investigated in the future using different turbulence length scales.

## 7. CONCLUSIONS AND FUTURE WORK

A Large Eddy Simulation of the CART-2 wind turbine blade section in an annular domain has been performed to estimate the far field noise due to unsteady aerodynamic loadings. The choice of the annular section is based on the acoustic field measurement by Oerlemans. The initial results are compared with field measurement data by Moriarty and show good agreement. This shows that acoustic noise estimates can be made with less computational expense than by performing full wind turbine simulations, and with higher accuracy than using semi-empirical noise prediction codes. Additionally, this work suggests that there is a limited effect on the acoustic sources of a rotational blade from the radial flow along the blade. The effects of turbulent length scales and trailing edge bluntness will be examined in future research.

## 8. ACKNOWLEDGEMENTS

The authors wish to acknowledge the University of Auckland Doctoral Scholarship, Young Professional Congress Attendance Grants for INTER-NOISE 2014 and the contribution of the NeSI high-performance computing facilities and the staff at the Centre for eResearch at the University of Auckland. New Zealand's national facilities are provided by the New Zealand eScience Infrastructure (NeSI) and funded jointly by NeSI's collaborator institutions and through the Ministry of Business, Innovation and Employment's Infrastructure programme. URL <http://www.nesi.org.nz>

## REFERENCES

1. Salt AN, Hullar TE. Responses of the ear to low frequency sounds, infrasound and wind turbines. *Hearing research*. 2010;268(1):12–21.
2. Nissenbaum MA, Aramini JJ, Hanning CD, et al. Effects of industrial wind turbine noise on sleep and health. *Noise and Health*. 2012;14(60):237.
3. Pinder N. Mechanical noise from wind turbines. *Wind Engineering*. 1992;16(3):158–167.
4. Tong W. *Wind power generation and wind turbine design*. WIT Press; 2010.
5. Williams JF, Hawkings DL. Sound generation by turbulence and surfaces in arbitrary motion. *Philosophical Transactions of the Royal Society of London Series A, Mathematical and Physical Sciences*. 1969;264(1151):321–342.
6. Lighthill MJ. On sound generated aerodynamically. I. General theory. *Proceedings of the Royal Society of London Series A Mathematical and Physical Sciences*. 1952;211(1107):564–587.
7. Oerlemans S, Schepers J, Guidati G, Wagner S. Experimental demonstration of wind turbine noise reduction through optimized airfoil shape and trailing-edge serrations. *National Aerospace Laboratory*. 2001;(324).
8. ANSYS Fluent 15.0 User's Guide. Ansys Inc; 2013.
9. Brooks TF, Schlinker RH. Progress in rotor broadband noise research. *Vertica*. 1983;7:287–307.
10. Brooks TF, Pope DS, Marcolini MA. *Airfoil self-noise and prediction*. vol. 1218. National Aeronautics and Space Administration, Office of Management, Scientific and Technical Information Division; 1989.
11. McAlpine A, Kingan MJ. Far-field sound radiation due to an installed open rotor. *International Journal of Aeroacoustics*. 2012;11(2):213–246.
12. Wagner S, Bareiss R, Guidati G, Wagner-Bareiß-Guidati. *Wind turbine noise*. 1996;.
13. Schlinker RH, Amiet RK. Helicopter rotor trailing edge noise. In: *AIAA, Astrodynamics Specialist Conference*. vol. 1. Lake Tahoe, Nevada, USA; 1981. .
14. Mo JO, Lee YH. Numerical simulation for prediction of aerodynamic noise characteristics on a HAWT of NREL phase VI. *Journal of mechanical science and technology*. 2011;25(5):1341–1349.
15. Arakawa C, Fleig O, Iida M, Shimooka M. Numerical approach for noise reduction of wind turbine blade tip with earth simulator. *Journal of the Earth Simulator*. 2005;2(3):11–33.
16. Moriarty P. Development and validation of a semi-empirical wind turbine aeroacoustic code. *NREL Report*. 2004;.
17. Wagner CA, Hüttl T, Sagaut P. *Large-eddy simulation for acoustics*. vol. 118. Cambridge University Press Cambridge; 2007.
18. Smagorinsky J. General circulation experiments with the primitive equations: I. The basic experiment. *Monthly weather review*. 1963;91(3):99–164.
19. Germano M, Piomelli U, Moin P, Cabot WH. A dynamic subgrid-scale eddy viscosity model. *Physics of Fluids A: Fluid Dynamics (1989-1993)*. 1991;3(7):1760–1765.
20. Lighthill MJ, Whitham GB. On kinematic waves. II. A theory of traffic flow on long crowded roads. *Proceedings of the Royal Society of London Series A Mathematical and Physical Sciences*. 1955;229(1178):317–345.
21. Ffowcs-Williams J, Hawkings D. Theory relating to the noise of rotating machinery. *Journal of Sound and Vibration*. 1969;10(1):10–21.
22. Farassat F. Linear acoustic formulas for calculation of rotating blade noise. *AIAA Journal*. 1981;19(9):1122–1130.
23. Farassat F. Derivation of Formulations 1 and 1A of Farassat. *NASA TM*. 2007;214853:2007.

24. Brentner KS. Prediction of helicopter rotor discrete frequency noise: a computer program incorporating realistic blade motions and advanced acoustic formulation. NASA TM 87721. 1986;1.
25. ANSYS ICEM CFD User's Manual. Ansys Inc; 2013.
26. Batinat JT, Branch UA, Yangi HT. Spatial adaption procedures on unstructured meshes for accurate unsteady aerodynamic flow computation. 1991;.
27. Welch PD. The use of fast Fourier transform for the estimation of power spectra: a method based on time averaging over short, modified periodograms. IEEE Transactions on audio and electroacoustics. 1967;15(2):70–73.
28. Abbott IH, Von Doenhoff A. Theory of wing sections, including a summary of airfoil data. Dover Publications; 1959.